Int. J. Electrochem. Sci., 12 **(2017)** 10616 – 10632, doi: 10.20964/2017.11.17

International Journal of
ELECTROCHEMICAL
SCIENCE
www.electrochemsci.org

Investigation on the Corrosion and Cavitation Erosion Behaviors of the Cast and Friction Stir Processed Ni-Al Bronze in Sulfide-Containing Chloride Solution

Q.N. Song[1], *N. Xu* [1], *W. Gu* [1], *Y.F. Bao* [1,*] , *C.Y. Wei*[1], *F.S. Ni*[1], *Y.G. Zheng*[2], *D.R. Ni*[2], *Y.X. Qiao*[3]

[1] Engineering Research Center of Dredging Technology of Ministry of Education, Hohai University, 200 Jinling North Road, Changzhou 213022, China
[2] Institute of Metal Research, Chinese Academy of Sciences, 62 Wenhua Road, Shenyang 110016, China
[3] College of Materials Science and Engineering, Jiangsu University of Science and Technology, 2 Mengxi Road, Zhenjiang 212003, China
[*]E-mail: baoyf@hhuc.edu.cn

Received: 26 June 2017 / *Accepted:* 23 August 2017 / *Published:* 12 October 2017

Corrosion and cavitation erosion behaviors of the cast and friction stir processed (FSP) Ni-Al bronze (NAB) in sulfide-containing (polluted) 3.5% NaCl solution were investigated in the present study. The electrochemical impedance spectroscopy (EIS) results demonstrated that the corrosion product film formed in the polluted solution was of poor protectiveness, and the gravimetric measurements results indicated that the sulfide ions increased the corrosion rate by a factor of 1.13 for the cast and 2.12 for the FSP NAB, compared with the results in clean 3.5% NaCl solution. The sulfide ions promoted the formation of a thick and porous corrosion product film, which consisted of sulfides and oxides. Deep pits were found propagated along the eutectoid microstructure for the cast and the β' phases for the FSP NAB. The cavitation erosion mass loss with the addition of sulfide was 0.92 times and 2.52 times more than that in the clean solution for the cast and FSP, respectively. The increased corrosion damage induced by the sulfide ions deteriorated the mechanical properties and consequently accelerated the cavitation erosion degradation. The corrosion-cavitation erosion synergy/total mass loss (i.e. S/T) value in the polluted solution reached 73.48% for the cast and 76.94% for the FSP. It can be seen that the FSP NAB exhibited no obvious superiority in the corrosion and cavitation erosion resistance, compared with the cast one in the sulfide-containing chloride solution.

Keywords: Friction stir processing; Ni-Al bronze; Sulfide; Corrosion; Cavitation erosion

1. INTRODUCTION

Cavitation erosion is a degradation mode which typically occurs on propellers, impellers, hydroturbines and pumps, etc [1]. In hydraulic environments, the pressure fluctuation in liquids results

in generation and burst of bubbles. The liquid adjacent to the bursting bubbles attacked on the components at a high speed and causes material degradation. Propellers are the key propulsion plant for ships in marine environment. Because of the long-term immersion and high-speed rotation in seawater, ship propellers experience both corrosion and cavitation erosion.

Ni-Al bronze (NAB), of nominal composition 9-12% Al, 6% Fe, 6% Ni and 2% Mn, is one of the main materials for making ship propellers because of the combination of high mechanical properties and excellent corrosion resistance [2]. Large-size NAB ship propellers, which are generally castings, contain inhomogeneous and coarse microstructure and casting porosities. These casting defects reduce the mechanical properties, corrosion and cavitation erosion resistance, and consequently shorten the lifetime of ship propellers. Friction stir processing (FSP) is an innovative surface technique which is derived from friction stir welding (FSW) [3], and it has been revealed to improve both the strength and ductility of the cast NAB by means of refining the cast microstructure and eliminating the casting porosities [4-7]. Recently, the corrosion, wear and cavitation erosion behaviors of the FSP NAB have also received consideration [8-11]. The results reveal that FSP is a promising surface method to enhance the above properties of the cast NAB in chloride solutions.

However, the discharged industrial wastes and metabolic process of marine creatures introduce various pollutants into seawater. The metabolism of marine organisms and microorganisms and the reduction of sulfide reducing bacteria (SRB) give rise to sulfide pollution of seawater. It has been revealed that the sulfide ions remarkably increase the corrosion rate of copper and its alloys [12-15]. In sulfide-containing seawater, copper sulfide was formed in the corrosion product film. It significantly accelerated the charge transfer kinetic of the oxygen reduction for the cast NAB and the corrosion rate depended sensitively on the high flow velocities [16]. Recently, the damage mechanism of a NAB canned motor pump impeller working in highly polluted seawater was analyzed, and it was found that the sulfide pollution in seawater resulted in severe selective phase corrosion of NAB and led to surface perforation through pitting mechanism. Cu-S-O corrosion products formed at the corroded areas because of the reaction between the sulfur and oxides [17]. For ship propellers, increased corrosion damage caused by the aggressive sulfide ions might also facilitate cavitation erosion degradation. To our knowledge, the influence of sulfide ions on the corrosion and cavitation erosion behaviors in chloride solution has been lack of research for the cast and FSP NAB.

In the present study, electrochemical and gravimetric measurements were performed to investigate the corrosion behavior of the cast and FSP NAB in sulfide-containing 3.5 % NaCl solution. Ultrasonically vibrating cavitation erosion tests were conducted to evaluate the cavitation erosion behavior. The corrosion product film has been characterized, and the synergism between corrosion and cavitation erosion have been analyzed.

2. EXPERIMENTAL

2.1. Materials

The investigated cast NAB with UNS designation C95800 contained 9.18% Al, 4.49% Ni, 4.06% Fe and 1.03% Mn. FSP was performed on cast NAB plates with a dimension of 300 mm × 70

mm × 8 mm. The stirring tool was made of a nickel-based alloy. The concave shoulder of the tool was 24 mm in diameter, and the threaded conical pin was 8 mm in root diameter and 7 mm in length. The rotating rate, traverse speed and tilt angle of the tool were 1,200 rpm, 50 mm/min and 3°, respectively. During FSP, blowing air was used to cool the tool and NAB plates.

2.2. Electrochemical measurements

Electrochemical measurements were conducted in a typical three-electrode system using a Gamry 1000E potentiostat. The working electrode was the cast or FSP NAB, the counter electrode was a platinum plate and the reference electrode was a saturated calomel electrode (SCE). The test media were 3.5 % NaCl solution and 3.5 % NaCl + 20 ppm Na_2S solution which were noted as the clean and polluted solution hereinafter. Analytical grade sodium chloride, sodium sulfide nonahydrate and distilled water were used for solution preparation. The reference electrode was connected with the test medium using a salt bridge. The sample was first immersed in the test medium for at least 30 min in order to obtain a stable potential. The electrochemical impedance spectroscopy (EIS) measurements were conducted at open circuit potential over a frequency domain from 100 kHz to 10 mHz, the AC amplitude perturbation voltage was 5 mV. The dynamic polarization tests were performed at a scan rate of 0.5 mV/s over a potential range from -0.5 V to 1.2 V versus open circuit potential. All the electrochemical measurements were conducted at least three times for each sample and in each solution to ensure the reproducibility.

2.3. Gravimetric measurements

The cast or FSP NAB with a dimension of 14 mm × 10 mm × 2 mm were prepared for the gravimetric measurements. Each sample was immersed in the clean or polluted solutions at room temperature (approximately 25°C). The polluted solution was refreshed daily because the sulfide concentration decreased with the exposing time to the air. After 15 days' immersion, the sample was transferred to a pickling solution for 2 minutes to wipe off the corrosion product film which formed in the test medium. The volume fractions of hydrochloric acid and distilled water in the pickling solution were both 50%. Negligible mass loss was caused during the pickling process for both the cast and FSP NAB substrates. The sample weights were recorded as m_0 for the initial weight before immersion, m_1 for the weight with film after immersion and m_2 for the weight with film removed. Thus, the mass loss of the sample and the weight of the corrosion product film equaled to m_0-m_2 and m_1-m_2, respectively. For each material, at least three samples were prepared in each solution to ensure the accuracy of the gravimetric measurements.

2.4. Cavitation erosion tests

Cavitation erosion tests were conducted in polluted solution using an ultrasonically vibrating device. The sample was held at a depth of 15 mm in the test medium and the vibrating horn was 0.5

mm right above the sample. The horn was vibrating at a frequency of 20 kHz and amplitude of 60 μm. Cycling cooling water was used to maintain the medium temperature at about 20°C. The mass loss was recorded after different periods. In order to analyze the synergism between corrosion and cavitation erosion in the polluted solution, the cavitation erosion mass loss results in distilled water and clean 3.5 % NaCl solution, which had already been studied in our previous study, were cited in the present study to make comparison [9]. All tests were done in accordance with ASTM G32 standard [18].

The surface and cross-section morphologies of the corroded and eroded cast and FSP NAB were observed by stereoscopy and scanning electron microscopy (SEM, JSM6510A). The composition of the corrosion product films were characterized by energy dispersive spectroscopy (EDS, JED 2300).

3. RESULTS AND DISCUSSION

3.1 Microstructure

Fig. 1 shows the optical microstructures of the cast and FSP NAB. As indicated in Fig. 1(a), the cast substrate consisted of lightly-etched Widmanstätten α phase and darkly-etched β' and κ phases. The microstructure of the FSP NAB had been previously characterized and analyzed in our studies [4, 9]. In the stirred zone, the microstructure varied along the plate thickness because different positions experienced different thermal and deformation histories. The equiaxed microstructure possessed most of the stirred zone in FSP NAB. Equiaxed α and β', along with a small portion of Widmanstätten α phases were distributed evenly, as presented in Fig. 1(b).

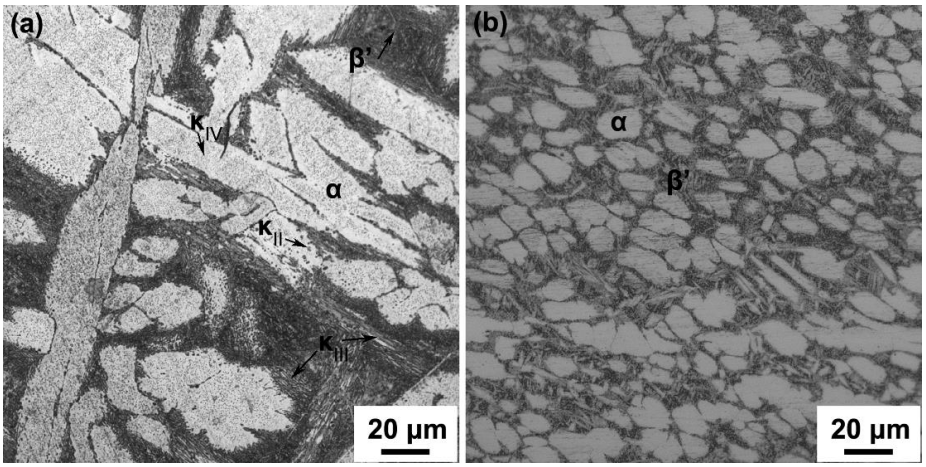

Figure 1. Optical microstructures of (a) cast and (b) FSP NAB

3.2 Corrosion behavior

3.2.1 Electrochemical measurement results

Fig. 2 shows the EIS results in the clean and polluted solutions of the cast and FSP NAB. The capacitance arc radius of the cast and FSP NAB were close in both solutions, indicating that the two

materials possessed similar corrosion resistance. The impedance data was fitted using Zsimpwin software.

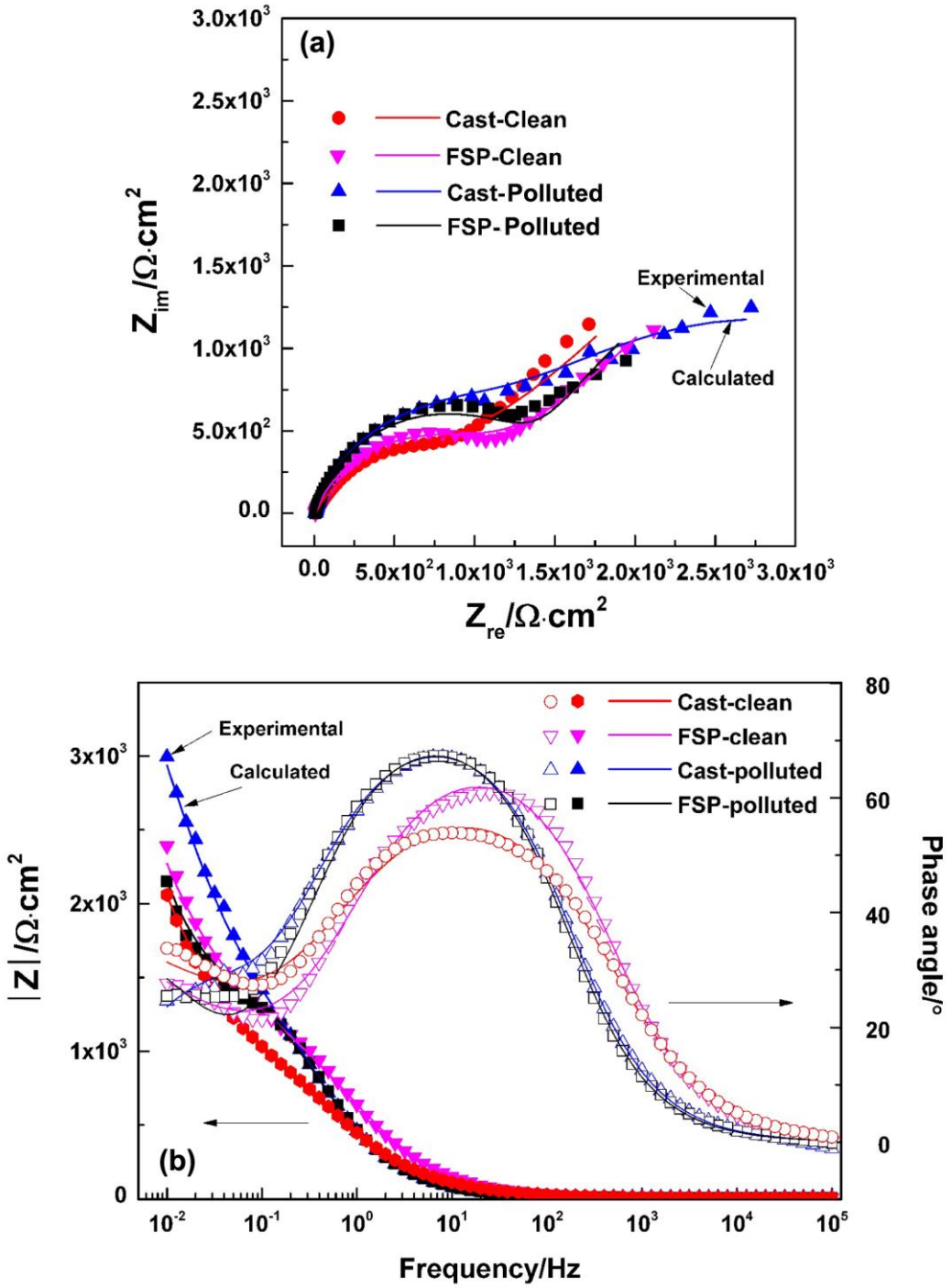

Figure 2. (a) Nyquist and (b) Bode plots of cast and FSP NAB in clean and polluted solutions

Fig. 3 presents the equivalent circuits used for fitting the EIS results. A constant phase element (CPE) is generally used instead of an ideal capacitance element in consideration of the surface heterogeneity of the electrode. The impedance of CPE equals to $[C(j\omega)^n]^{-1}$, where C is the capacitance,

j is the imaginary number, ω is the angular frequency and n is an adjusting factor which describes a frequency dispersion of time constants because of surface heterogeneities. The equivalent circuit (a) was used to fit the EIS result in the clean solution, and Warburg impedance, W was introduced to represent the diffusion process upon immersion in the newly-prepared 3.5% NaCl solution. C_1 was the capacitance of the double electric layer at the metal/solution interface. R_{ct} was the charge transfer resistance. It was noted that upon immersion in the polluted solution, both the cast and FSP NAB surfaces turned black soon, and the capacitance arc radius was also larger than that in the clean solution because of the formation of copper sulfides. In consideration of the defective and porous structure of the film, equivalent circuit (b) was used for EIS results in the polluted solution [13]. C_2 and R_f represented the capacitance and resistance characters of the film. The electrochemical parameters were listed in Table 1. The fitting quality was evaluated by the Chi-square (χ^2) value. In the polluted solution, the R_{ct} value was 3.066 k$\Omega\cdot$cm^2 for the cast and 4.57 k$\Omega\cdot$cm^2 for the FSP, which was higher than that in the clean solution (1.018 k$\Omega\cdot$cm^2 for the cast and 1.126 k$\Omega\cdot$cm^2 for the FSP), indicating that the quick film formation in presence of sulfide increased the charge transfer resistance. The film resistance, R_f, reached 1.571 k$\Omega\cdot$cm^2 for the cast and 1.514 k$\Omega\cdot$cm^2 for the FSP.

Fig. 4 shows the polarization curves. It can be seen that the cast and FSP experienced similar cathodic and anodic processes in both solutions. In the polluted solution, the cathodic process was slower for both the two materials, compared with the result in the clean solution. The cathodic process was suppressed and the corrosion current density decreased as a result of the film formation. As seen in the magnification part of Fig. 4, there existed a current density peak at about -0.275 V in the polarization curve which corresponded to the formation of cuprous oxide [19]. Therefore, the corrosion rate was kept at a low value and the two materials exhibited a passive behavior. However, such a current density peak disappeared in the polluted solution. With the addition of sulfide ions, the corrosion product films formed on the two materials contained sulfides, in addition to the oxides [13]. The mixture of sulfides and oxides was less compact and protective than that of the oxides [20], therefore with increasing the applied potential, the current density progressively increased, and no obvious passivation was found.

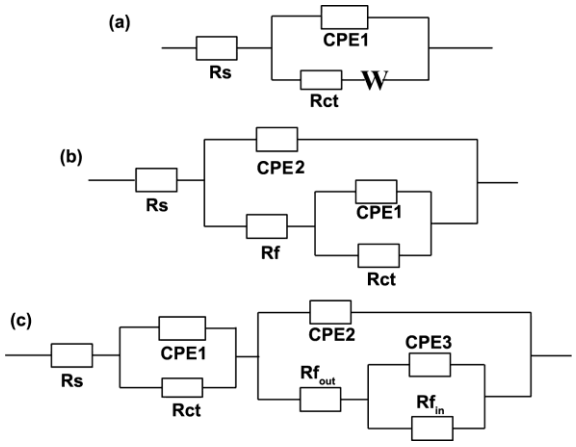

Figure 3. Equivalent circuits used for fitting the EIS results: (a) for cast NAB after initial immersion in the clean solution; (b) for FSP NAB after initial and long-term immersion in the polluted solution; (c) for cast and FSP NAB after long-term immersion in the clean solution.

Table 1. Electrochemical parameters of cast and FSP NAB upon immersion in clean and polluted solutions

Material/solution		Cast/clean	FSP/clean	Cast/polluted	FSP/polluted
Parame-ters	R_s($\Omega\cdot cm^2$)	8.021	7.686	7.259	7.622
	R_{ct}($k\Omega\cdot cm^2$)	1.018	1.126	3.066	4.570
	C_1($\mu F\cdot cm^{-2}$)	466.4	251.2	2,588	7,686
	n_1	0.7032	0.782	0.716	0.8103
	W	0.002703	0.002763	-	-
	R_f($k\Omega\cdot cm^2$)	-	-	1.571	1.514
	C_2($\mu F\cdot cm^{-2}$)	-	-	413.6	410.9
	n_2	-	-	0.8271	0.8328
	$\sum\chi^2$	6.49×10^{-4}	5.771×10^{-4}	2.56×10^{-4}	8.71×10^{-4}

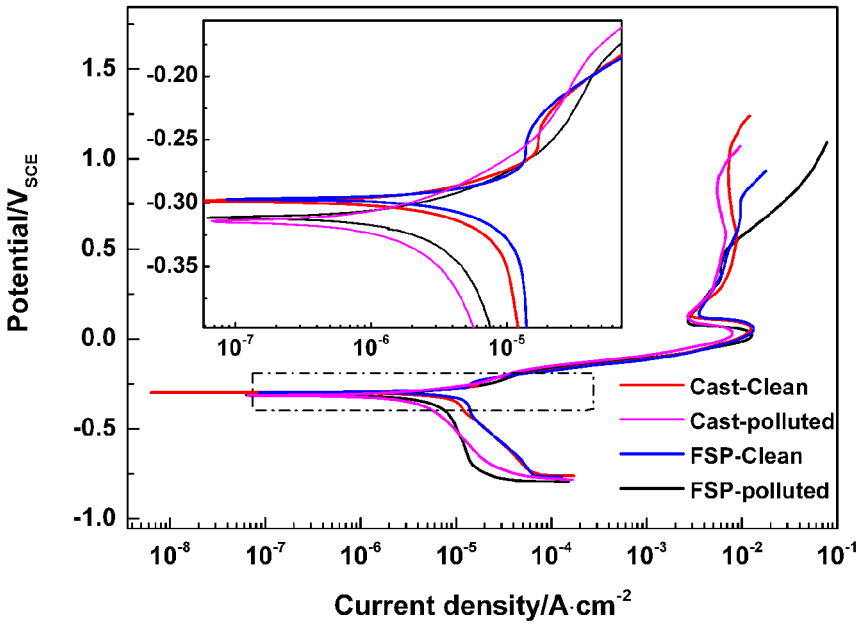

Figure 4. Polarization curves of cast and FSP NAB in clean and polluted solutions

EIS measurements were also performed on the cast and FSP NAB which were immersed in the clean and polluted solutions for a long period in order to evaluate the protectiveness of the corrosion product films. Fig. 5 shows the EIS results. Equivalent circuit (c) in Fig. 3 was used to fit the EIS result in the clean solution, where a duplex oxide film was formed. The film consisted of a defective and porous outer layer and a compact inner layer [13]. C_2/R_{fout} and C_3/R_{fin} represented the capacitance/resistance of the outer and inner layers of the film, respectively. The electrochemical parameters results are listed in Table 2. After long-term immersion in the clean solution, a protective film formed on both the cast and FSP NAB and acted as a barrier against the corrosive chloride ions. The R_{ct} value reached 11.2 and 52.24 $k\Omega\cdot cm^2$ for the cast and FSP NAB, respectively. The R_{fout} value was very low, while the R_{fin} value was 7.2 $k\Omega\cdot cm^2$ for the cast and 19.45 $k\Omega\cdot cm^2$ for the FSP. In

addition, the capacitance of the inner layer, C_3, was much lower than that of the outer layer, indicating that the inner layer was more compact and protective than the outer layer. It can be seen that the film on FSP NAB was much more protective, and this was discussed in detail in our previous study [9]. Because of the porous structure of the film in the polluted solution, equivalent circuit (b) in Fig. 3 was also used to fit the EIS result after long-term immersion [13]. The R_{ct} value was 2.043 and 1.559 kΩ·cm^2 for the cast and FSP NAB, respectively. The R_f value was only 0.12 kΩ·cm^2 for the cast and 0.102 kΩ·cm^2 for the FSP. It can be seen that both R_{ct} and R_f decreased after long-term immersion, compared with the results at the initial immersion stage shown in Table 1. This result demonstrated that the film formed in the polluted solution was nearly non-protective. The sulfide ions acted as a catalyst to facilitate both the anodic and cathodic reactions for copper and its alloys [13], therefore the R_{ct} value was very low.

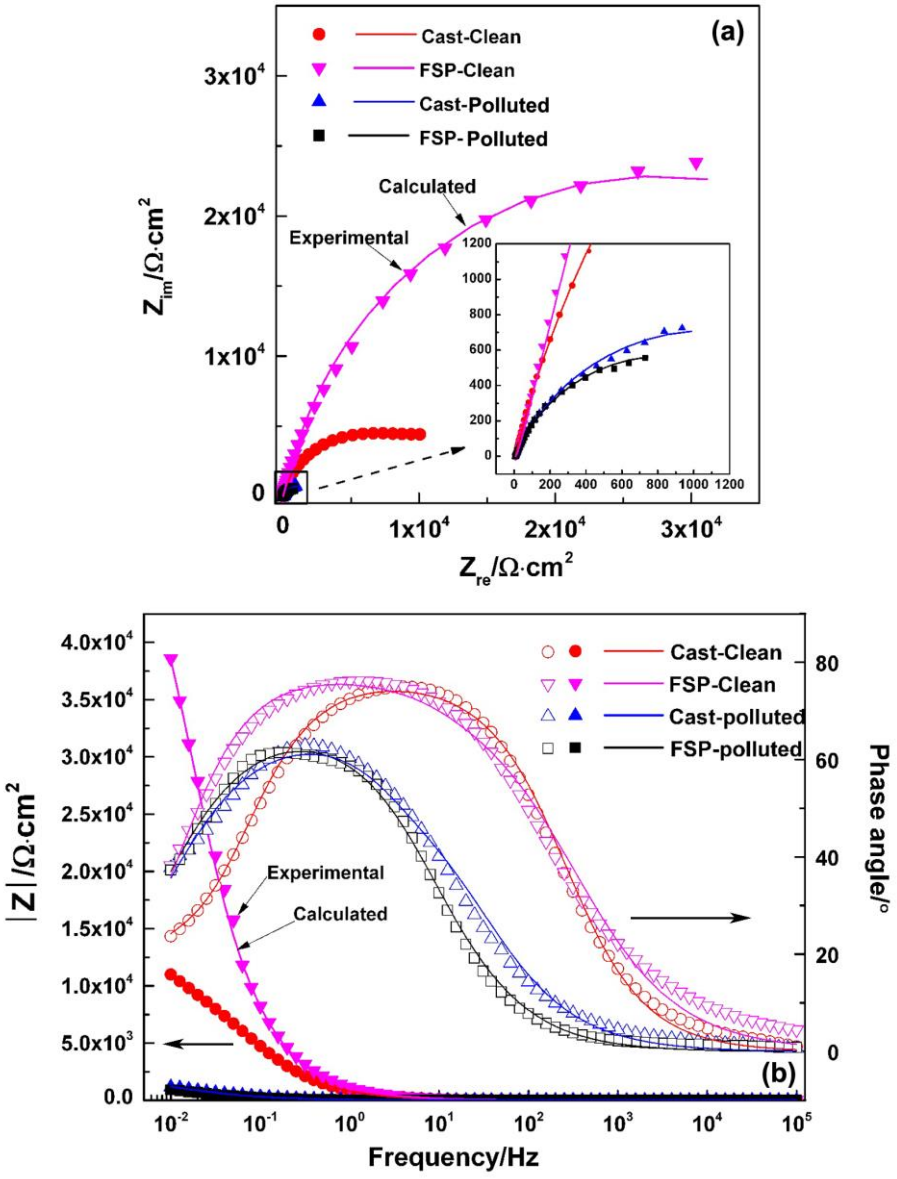

Figure 5. EIS results of cast and FSP NAB after immersion for 15 days in clean and polluted solutions

Table 2. Electrochemical parameters results of cast and FSP NAB after immersion in clean and \polluted solutions for 15 days

Material/solution		Cast/clean	FSP/clean	Cast/polluted	FSP/polluted
Parame -ters	R_s($\Omega\cdot cm^2$)	7.255	8.84	6.65	7.573
	R_{ct}($k\Omega\cdot cm^2$)	11.2	52.24	2.043	1.559
	C_1($\mu F\cdot cm^{-2}$)	1,500	192.1	443	124
	n_1	0.76	0.895	0.91	0.91
	R_f	-	-	0.120	0.102
	R_{fout}($k\Omega\cdot cm^2$)	0.422	0.245	-	-
	C_2($\mu F\cdot cm^{-2}$)	291.6	1,950	3,748	5,695
	n_2	0.88	0.57	0.73	0.76
	R_{fin}($k\Omega\cdot cm^2$)	7.2	19.45	-	-
	C_3($\mu F\cdot cm^{-2}$)	5.526	127.1	-	-
	n_3	0.87	0.87	-	-
	$\sum\chi^2$	1.368×10^{-3}	4.268×10^{-3}	1.78×10^{-3}	6.978×10^{-4}

3.2.2 Gravimetric measurement results

Fig. 6 shows the gravimetric measurement results in the clean and polluted solutions. After 15 days' immersion, the corrosion mass loss rates of the cast and FSP NAB were 0.0023 $mg\cdot cm^{-2}\cdot h^{-1}$ and 0.0017 $mg\cdot cm^{-2}\cdot h^{-1}$ in the clean solution, respectively. However, the corrosion mass loss rate reached 0.0049 $mg\cdot cm^{-2}\cdot h^{-1}$ for the cast NAB and 0.0053 $mg\cdot cm^{-2}\cdot h^{-1}$ for the FSP one in the polluted solution. Namely, the addition of sulfide ions raised the corrosion rate by a factor of 1.13 for the cast and 2.12 for the FSP NAB. Fig. 6 also showed that the weight of the corrosion product film was much larger in the presence of sulfide, indicating the formation of a much thicker film. However, the film possessed poor protectiveness according to the mass loss result. The gravimetric measurement results were consistent with the EIS results shown in Fig. 5.

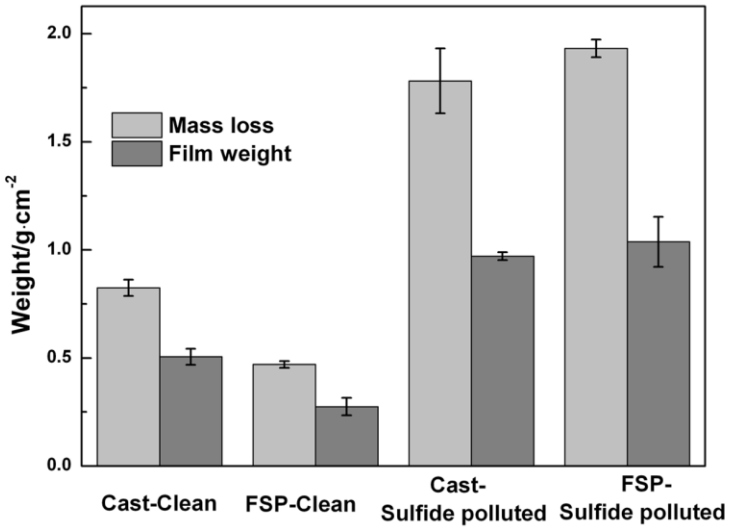

Figure 6. Gravimetric measurement results of the cast and FSP NAB after 15 days' immersion in clean and polluted solutions.

3.3 Film characterization

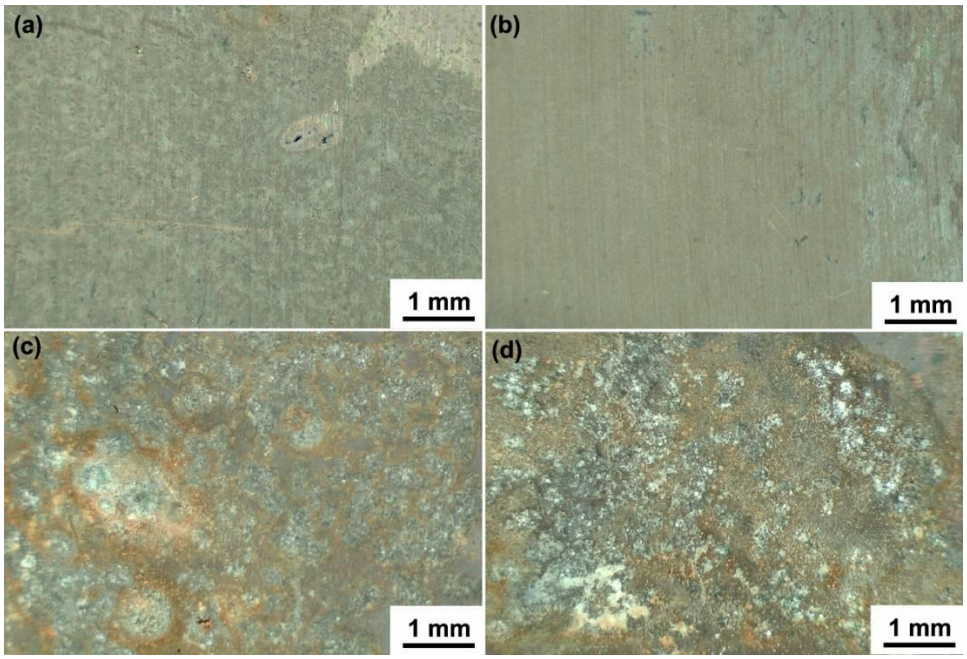

Figure 7. Stereoscopic morphologies of cast and FSP NAB after 15 days' immersion in clean and polluted solutions: (a) Cast, clean; (b) FSP, clean; (c) Cast, polluted; (d) FSP, polluted.

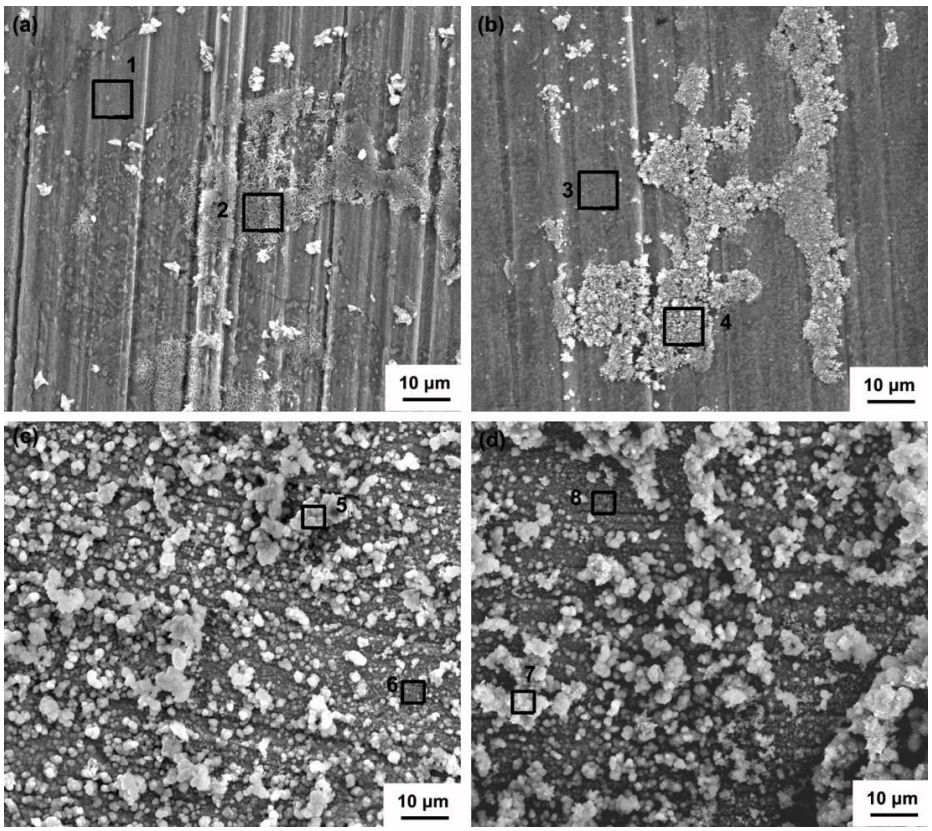

Figure 8. Surface morphologies of cast and FSP NAB obtained by SEM after 15 days' immersion in clean and polluted solutions: (a) Cast, clean; (b) FSP, clean; (c) Cast, polluted; (d) FSP, polluted.

Fig. 7 shows the stereoscopic surface morphologies. The corrosion product films formed on the cast and FSP NAB in the polluted solution were definitely different from those in the clean solution. Much thicker corrosion products covered the surface in the polluted solution. It can be seen that the sulfide ions influenced corrosion behavior by changing both the structure and composition of the film.

Fig. 8 shows the surface morphologies obtained by SEM, and Table 3 presents the EDS results of different corrosion products. In the clean solution, the film was thin and the microstructure of the cast and FSP substrate was visible, as shown in Figs. 8(a) and 8(b). Porous corrosion products were found discontinuously distributed on the outer layer of the film. Based on the EDS result and combining with our previous study, the inner layer mainly consisted of oxides, including Al_2O_3 and Fe/Ni incorporated Cu_2O. The outer layer contained higher chlorine content, indicating the existence of chlorides, such as $Cu_2(OH)_3Cl$ and Cu(OH)Cl [21]. Since FSP refined and homogenized the cast microstructure and eliminated the casting porosities, the film formed on the FSP NAB was more compact and protective than that on the cast one [9, 21]. Therefore, FSP exhibited superior corrosion resistance, as also proved by the EIS results shown in Fig. 5 and Table 2.

In the polluted solution, the inner layer of the film covered the whole substrate and the outer layer consisted of larger-size corrosion products which were distributed discontinuously, as shown in Figs. 8(c) and 8(d). According to the EDS result, sulfur was detected in both the inner and outer layer, demonstrating the formation of sulfides in addition to the oxides inside the film. It was reported that the sulfide interfered with the normal formation of an oxide film, and promoted the growth of a film which consisted of oxides and sulfide compounds, including Cu_2O, CuS and Cu_2S for copper and its alloys. The sulfides rendered the film defective, porous and reduced the film protectiveness [12, 13, 20]. Therefore, the corrosion rate of both the as-cast and FSP NAB increased with the addition of sulfide ions. It was also noteworthy that the Al content was up to 20 % in the outer layer and it was much higher than that in the substrate (approximately 9 %). The Fe content also reached up to 10% in the outer layer for the cast NAB, while it was approximately 5 % in the substrate. The Cu content was rather low in the film.

Table 3. Composition results of different corrosion products on the cast and FSP NAB surface shown in Fig. 8

Element (wt.%)		O	Cl	S	Al	Ni	Fe	Mn	Cu
Regions	1	19.01	0.23	-	8.62	7.06	9.45	1.66	53.98
	2	33.96	3.63	-	10.70	9.64	7.22	0.77	34.07
	3	20.25	1.49	-	10.68	9.26	8.04	1.47	48.82
	4	33.46	3.10	-	11.31	6.43	5.93	0.80	38.97
	5	58.44	1.25	3.41	20.05	0.19	10.00	0.20	6.46
	6	14.81	1.24	6.00	9.47	8.80	6.58	0.86	52.23
	7	63.91	1.28	2.17	22.63	0.65	5.59	0.04	3.57
	8	12.08	0.68	5.78	2.22	5.56	6.57	1.16	65.96

Fig. 9 shows the cross-section morphologies after 15 days' immersion in the clean and polluted solutions. In the clean solution, the FSP NAB suffered general corrosion (Fig. 9(b)), while corrosion pits with a depth of about 4.3 μm were found for the cast one (Fig. 9(a)). While in the polluted

solution, the corrosion pits extended deeply into the substrate for both the cast and FSP NAB. For the FSP NAB, it was the β' phase that suffered preferential corrosion damage (Fig. 9(d)), and the corrosion pits seemed to propagate along the α/β' phase boundaries with a depth of 21 μm. As shown in Fig. 9(c), severe corrosion occurred at the κ_{II} and eutectoid microstructure $\alpha+\kappa_{III}$ for the cast NAB. The corrosion pits extended along these microstructures and reached a depth of approximately 55 μm. It was noted that severe selective phase corrosion occurred for both the two materials. For the cast NAB, the κ_{II} and κ_{III} were intermetallics based on Fe_3Al and NiAl, respectively [22]. For the FSP NAB, many small-sized phases distributed inside the β' phases and they were rich in Fe, Ni and Al. Due to the dissolution of these phases, the corrosion product film contained large contents of these elements, as also detected by EDS. Namely, the selective phase corrosion at Fe and Al-rich phases resulted in deep corrosion pits and high corrosion rate in the presence of sulfide.

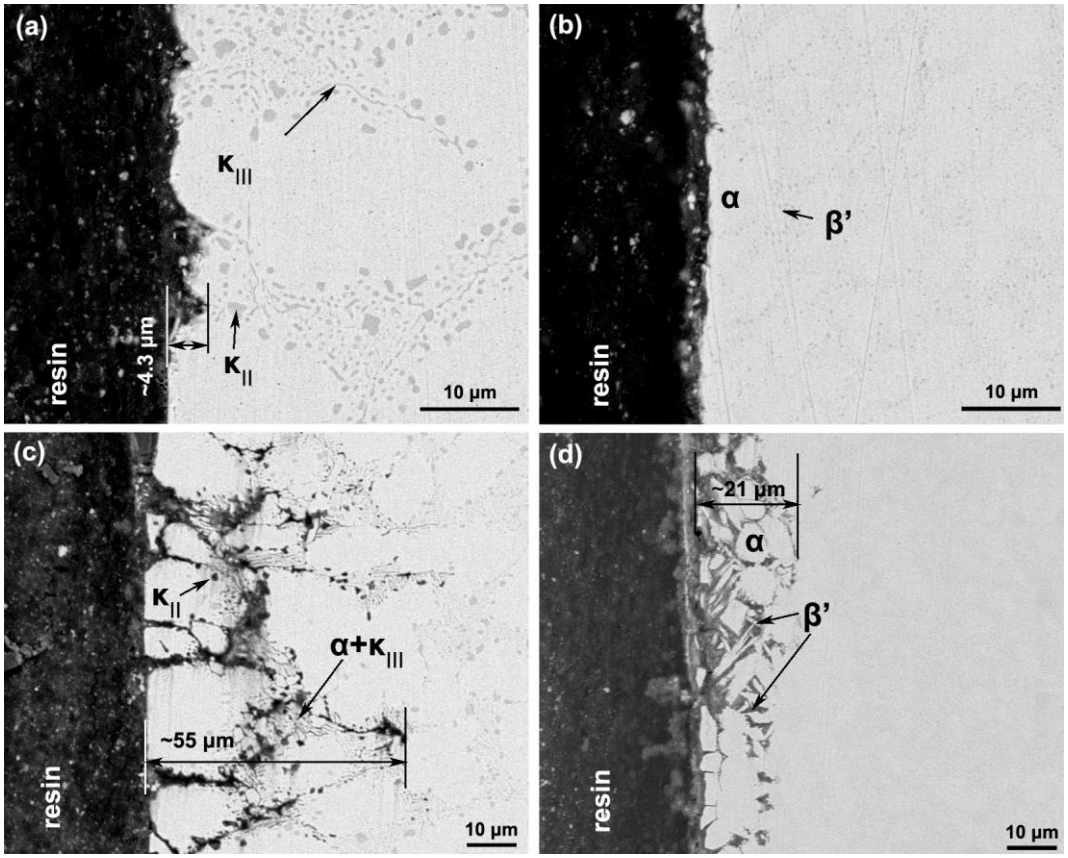

Figure 9. Cross-section morphologies of cast and FSP NAB after 15 days' immersion in clean and polluted solutions: (a) Cast, clean; (b) FSP, clean; (c) Cast, polluted; (d) FSP, polluted.

3.4 Cavitation erosion behavior

Fig. 10 shows the cavitation erosion mass loss results in the clean and polluted solutions. After cavitation erosion for 9 h in the clean solution, the mass loss rates of the cast and FSP NAB were 1.1728 $mg \cdot cm^{-2} \cdot h^{-1}$ and 0.5309 $mg \cdot cm^{-2} \cdot h^{-1}$ respectively [9]. In the polluted solution, the mass loss rate reached up to 2.2531 $mg \cdot cm^{-2} \cdot h^{-1}$ for the cast NAB and 1.8704 $mg \cdot cm^{-2} \cdot h^{-1}$ for the FSP one. It can be seen that the addition of sulfide ions raised the mass loss rate by 0.92 times for the cast and 2.52 times

for the FSP, compared with the results in the clean solution. When cavitation erosion took place in corrosive media, corrosion damage and the mechanical degradation caused by cavitation erosion would promote each other. Generally, the total mass loss was larger than the sum of the mass loss caused by pure cavitation erosion and pure corrosion. The total mass loss rate T, pure cavitation erosion rate E, pure corrosion rate C and synergy between corrosion and cavitation erosion S followed the equation as,

$$T = E + C + S \quad (1)$$

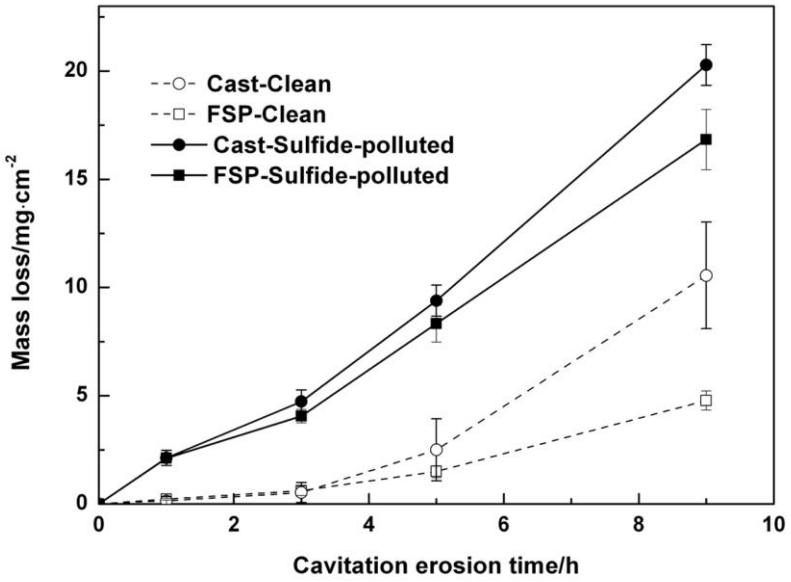

Figure 10. Cumulative cavitation erosion mass loss results of cast and FSP NAB in clean and polluted solutions

Table 4 shows the synergism analysis result. The pure cavitation erosion rate was obtained from the cavitation erosion test results in distilled water [9], and the pure corrosion rate was obtained from the gravimetric measurement results. In the clean solution, the S/T value of the cast NAB was 49.28%, and it was higher than that of the FSP one (19.53%). For both the two materials, the mechanical deterioration factor dominated the cavitation erosion mechanism. However, the cavitation erosion-corrosion synergy factor dominated the cavitation erosion degradation mechanism in the polluted solution. The S/T value reached up to 73.48% for the cast and 76.94% for the FSP.

Table 4. Cavitation erosion-corrosion synergism analysis result of the cast and FSP NAB in clean and polluted solutions

Material/solution	Mass loss rate ($mg \cdot cm^{-2} \cdot h^{-1}$)				Percentages (%)	
	T	*E*	*C*	*S*	*E/T*	*S/T*
Cast/Clean	1.1728	0.5926	0.0023	0.5779	50.53	49.28
FSP/Clean	0.5309	0.4259	0.0013	0.1037	80.22	19.53
Cast/Sulfide-polluted	2.2531	0.5926	0.0049	1.6556	26.30	73.48
FSP/Sulfide-polluted	1.8704	0.4259	0.0054	1.4391	22.77	76.94

Since FSP improved the strength remarkably and also increased the ductility of the cast NAB [4], the mass loss of the cast was much lower than that of the FSP in the clean solution, where mechanical damage factor dominated the cavitation erosion mechanism. However, it was found from Fig. 9 that corrosion pits propagated deeply into the substrate along the α/β' phase boundaries for the FSP and eutectoid microstructure for the cast in the polluted solution. The corrosion pits would reduce the mechanical properties of the surface and consequently increased the mass loss under cavitation erosion. Namely, the increased corrosion damage caused by the aggressive sulfide ions further promoted the cavitation erosion degradation. Therefore, the synergy extremely increased. It was also reported that the addition of sulfide ions accelerated the corrosion wear damage of copper alloys in seawater and microfracture dominated the failure of the worn surface [23].

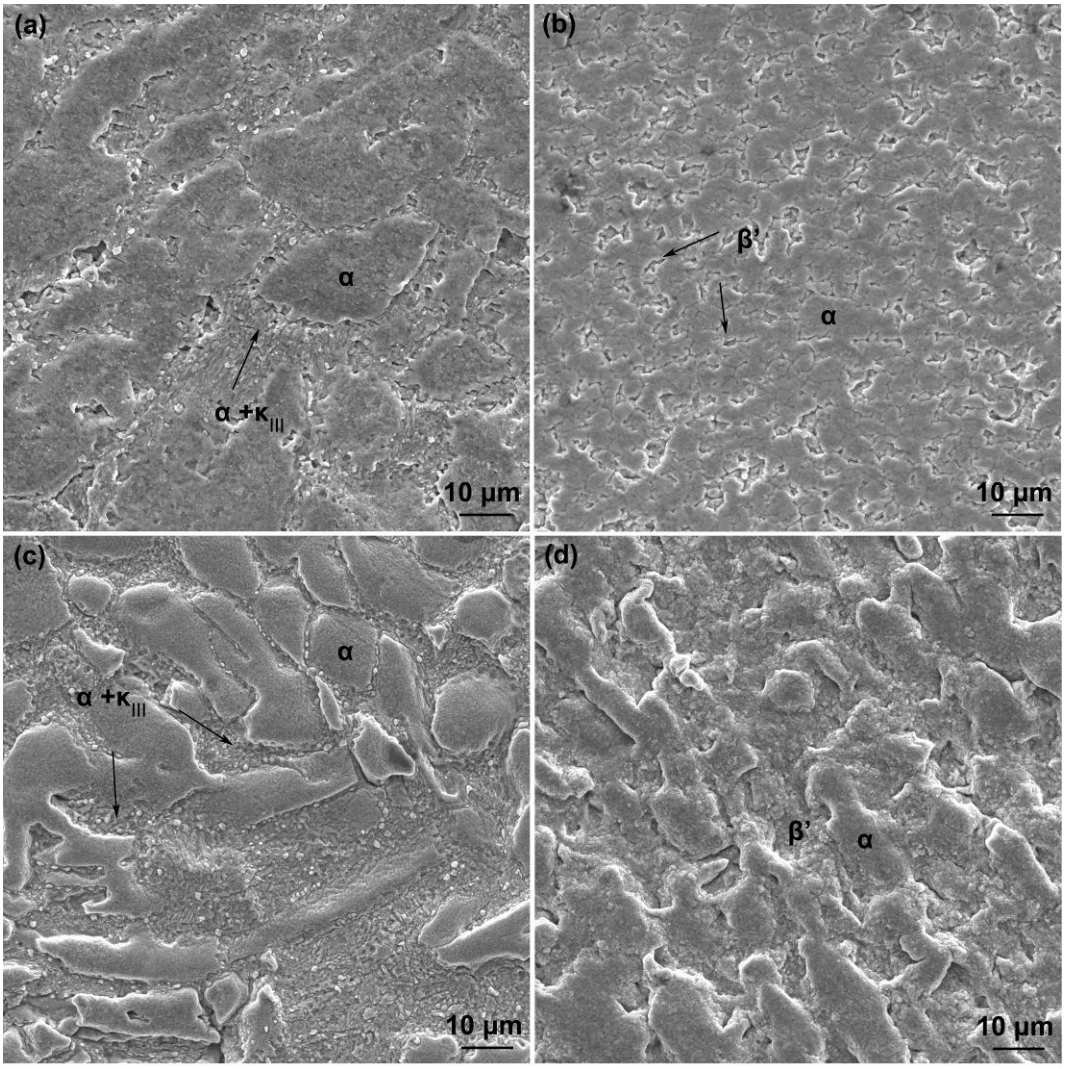

Figure 11. Surface morphologies of cast and FSP NAB after cavitation erosion for 1 h in clean and polluted solutions: (a) Cast, clean; (b) FSP, clean; (c) Cast, polluted; (d) FSP, polluted.

Figs. 11 and 12 show the surface morphologies after cavitation erosion for different time in the clean and polluted solutions. After 1 h in the clean solution, as shown in Figs. 11(a) and 11(b), the eutectoid microstructure α + κ_{III} for the cast NAB and β' phases for the FSP NAB were preferentially

corroded. Small and shallow cavities were also found on the surface. Because of the inhomogeneous microstructure, more galvanic corrosion sites existed on the cast NAB. Thus, more severe corrosion occurred (Fig. 9(a)) and resulted in higher corrosion-cavitation erosion synergy for the cast NAB. However, both the two materials suffered much more severe cavitation erosion damage in the polluted solution. As demonstrated in Figs. 11(c) and 11(d), the eutectoid microstructure of the cast and β' phases of the FSP NAB severely dissolved, resulting in much larger surface roughness. After cavitation erosion for 3 h in the clean solution, deep cavities were found on the cast NAB (Fig. 12(a)), and cavitation erosion attack extended to more areas of the surface for the FSP (Fig. 12(b)). In the sulfide-polluted solution, much larger and deeper cavities were found for the cast, as seen in Fig. 12(c). Exfoliation seemed to occur on the surface, leaving wide cavities for the FSP NAB, as seen in Fig. 12(d).

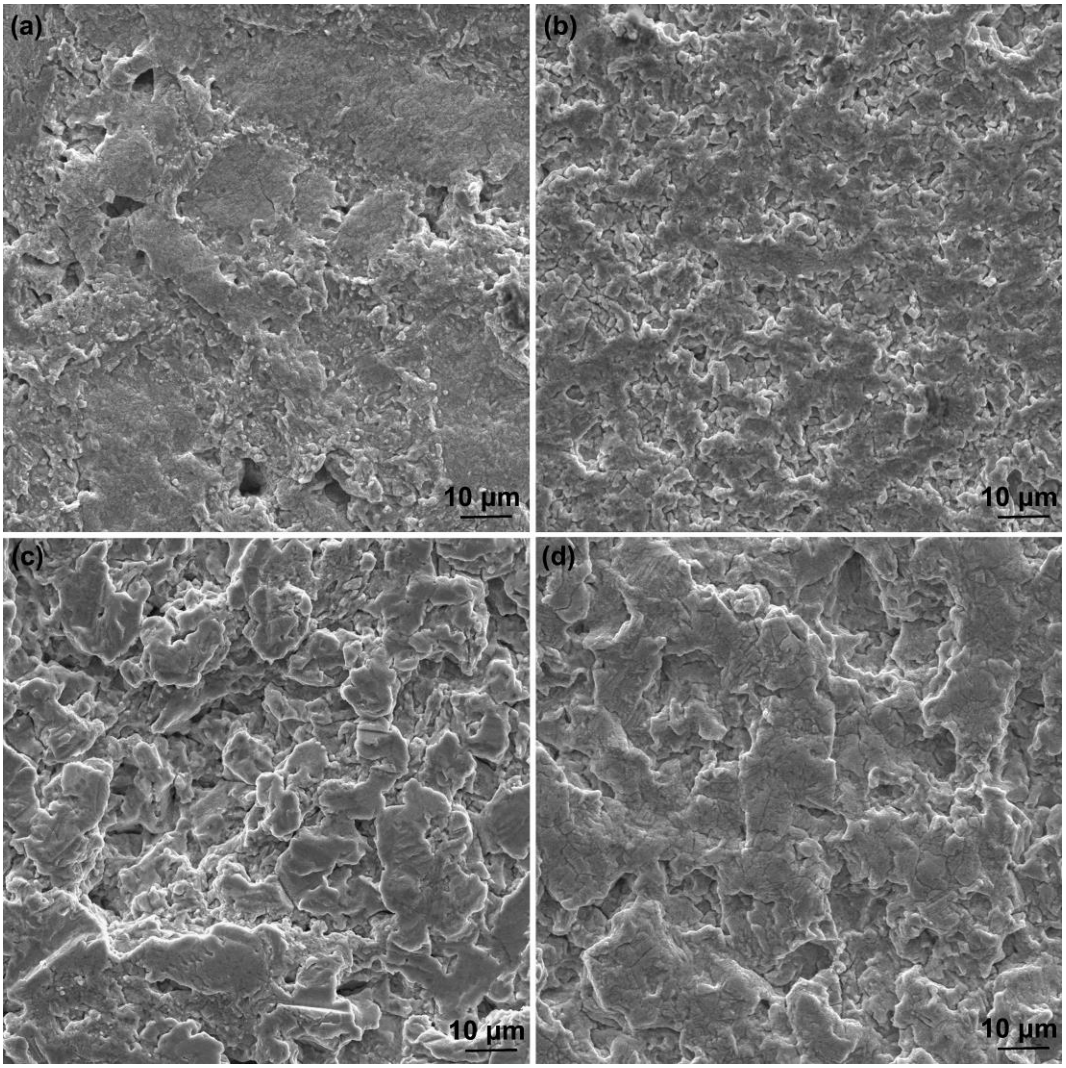

Figure 12. Surface morphologies of the cast and FSP NAB after cavitation erosion for 3 h in clean and polluted solutions: (a) Cast, clean; (b) FSP, clean; (c) Cast, polluted; (d) FSP, polluted.

From the above results, both the cast and FSP NAB suffered severe selective phase corrosion in the polluted solution. The remarkable cavitation erosion-corrosion synergy promoted the cavitation

erosion degradation significantly. It can be seen that the FSP NAB exhibited no obvious superiority in both the corrosion and cavitation erosion resistance in sulfide-containing chloride solution, compared with the cast one.

4. CONCLUSIONS

(1) Electrochemical results demonstrated that a much less protective corrosion product film formed in the polluted solution, compared with that in the clean solution. Gravimetric measurement results indicated that the presence of sulfide ions raised the corrosion rate by a factor of 1.13 for the cast and 2.12 for FSP NAB. Corrosion pits propagated deeply into the substrate along the eutectoid microstructure for the cast and the β' phases for the FSP NAB.

(2) The sulfide ions promoted the growth of a thicker and more porous film which consisted of both oxides and sulfides.

(3) The sulfide ions increased the cavitation erosion mass loss rate by 0.92 times for the cast and 2.52 times for the FSP NAB. The S/T value reached 73.48% for the cast and 76.94% for the FSP in the polluted solution.

(4) In the sulfide-polluted solution, FSP NAB suffered severe corrosion. The corrosion damage deteriorated the mechanical properties and consequently increased the cavitation erosion damage significantly. Therefore, the FSP NAB exhibited no obvious superiority in the corrosion and cavitation erosion resistance, compared with the cast one.

ACKNOWLEDGEMENTS
This research was financially supported by Fundamental Research Funds for the Central Universities of P.R. China (No. 2015B30314) and National Natural Science Foundation of China (No. 51601058 and 51401092).

References

1. A. Alhashem, P.G. Caceres, W.T. Riad and H.M. Shalaby, *Corrosion*, 51 (1995) 331.
2. J.A. Wharton, R.C. Barik, G. Kear, R.J.K. Wood, K.R. Stokes and F.C. Walsh, *Corros. Sci.*, 47 (2005) 3336.
3. W.M. Thomas, E.D. Nicholas, J.C. Needham, M.G. Murch, P. Temple–Smith and C.J. Dawes, G.B. Patent Application, No. 9125978.8,1991 (1991).
4. D.R. Ni, P. Xue, D. Wang, B.L. Xiao and Z.Y. Ma, *Mater. Sci. Eng*. A, 524 (2009) 119.
5. K. Oh-Ishi and T.R. McNelley, *Metall Mater. Trans*. A, 36A (2005) 1575.
6. W.A. Palko, R.S. Fielder and P.F. Young, *Mater. Sci. Forum*, 426-432 (2003) 2909.
7. Y. Lv, Y. Ding, Y. Han, L.-C. Zhang, L. Wang and W. Lu, *Mater. Sci. Eng*. A, 685 (2017) 439.
8. D.R. Ni, B.L. Xiao, Z.Y. Ma, Y.X. Qiao and Y.G. Zheng, *Corros. Sci*., 52 (2010) 1610.
9. Q.N. Song, Y.G. Zheng, S.L. Jiang, D.R. Ni and Z.Y. Ma, *Corrosion*, 69 (2013) 1111.
10. A. Ahmad, H. Li, Z. Pan, D. Cuiuri, S. Van Duin, N. Larkin, J. Polden and N. Lane, *Metall. Mater. Trans.* B, 45 (2014) 2291.
11. S. Thapliyal and D.K. Dwivedi, *Tribol. Int*., 97 (2016) 124.

12. K. Rahmouni, M. Keddam, A. Srhiri and H. Takenouti, *Corros. Sci*., 47 (2005) 3249.
13. S.J. Yuan and S.O. Pehkonen, *Corros. Sci*., 49 (2007) 1276.
14. Z. Mountassir and A. Srhiri, *Corros. Sci*., 49 (2007) 1350.
15. J.N. Al-Hajji and M.R. Reda, *Corros. Sci*., 34 (1993) 163.
16. A. Schussler and H.E. Exner, *Corros. Sci*., 34 (1993) 1803.
17. M. Hazra and K.P. Balan , *Eng. Fail. Anal*., 70 (2016) 141.
18. ASTM International G 32-03, 2003.
19. A.M. Alfantazi, T. M. Ahmed and D. Tromans, *Mater. Des*., 30 (2009) 2425.
20. N.K. Awad, E.A. Ashour and N.K. Allam, *Appl. Surf. Sci*., 346 (2015) 158.
21. Q.N. Song, Y.G. Zheng, D.R. Ni and Z.Y. Ma, *Corrosion*, 71 (2015) 606.
22. A.J. F. Hasan, G.W. Lorimer and N. Eidley, *Metall. Trans*. A, 13A (1982) 1337.
23. S.Z. Li, X. X. Jiang, H.Y. Bi and S. Li, *Wear*, 225–229 (1999) 1025.